ISBN: 978-3-95450-204-2 ISSN: 2673-5350 doi:10.18429/JACoW-IBIC2019-TUPP007

TRANSVERSE PHASE SPACE SCANNER DEVELOPMENTS AT IPHC

F. Osswald†, T. Adam, P. Graehling, M. Heine, C. Maazouzi, E. Traykov, Université de Strasbourg, IPHC, CNRS, UMR7178, 23 rue du Loess 67037 Strasbourg, France

Abstract

The Emittance characterization of charged particle beams is a standard and important tool to assess the performances of a facility. Due to emittance growth, beam losses, space charge and their incidence on beam matching and transport, the accurate measurement of the transverse phase space distribution of the charged particles is still an up-to-date issue. It enables detailed characterization of particle position and incidence distributions in addition to centroid position, profile, beam current and sectional shape measurement. It gives access to the particles distribution of the halo, a region of lower density important for high power accelerators and high intensity radioactive beams as they request reduced losses and damages thus less contaminated parts and nuclear waste for safe handling. Transverse phase space scanners are designed at IPHC and based on the Allison principle. They are currently used on different injection channels of large facilities as SPIRAL 2 and FAIR and will be used in the future on the DC280-SHE facility at JINR. A review of the IPHC's high resolution scanner design, development programme and future challenges are presented especially for beam halo analysis and "loss less" beam transport lines.

INTRODUCTION

The transverse phase scanner has been initially developed at IPHC in the 2000s for the SPIRAL 2 project then for FAIR with CEA-IRFU [1-5]. It is dedicated to low- energy ion-beam characterization. It is a slit-slit system based on Allison principle [6]. Each beamlet sampled by the entrance slit is analysed according to its incidence angle and energy. The analysis is performed by an electrostatic deflector composed of two parallel plates and a simple relation links the applied voltage to the angle. The beamlet current intensity is measured with a Faraday cup located after an exit slit. Another emittance-meter based on a slit-grid system has been developed at IPHC in the 80s and guided probably later choices [7].

DESIGN PARAMETERS

The main design parameters of the transverse phase scanner in Fig. 1 are shown in Table 1. To note that maximum beam size is 80 mm in diameter, beam power is limited to 300 W in DC mode and can be increased with duty cycle and defocusing of beam thus by decreasing the power density. The beam current intensity is fixed to the range between 10 µA and 3 mA in accordance with the characteristics of the front-end electronics i.e. the current-voltage convertor.

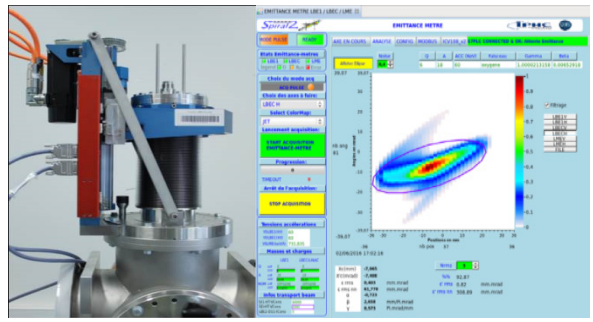

Figure 1: Transverse phase scanner mounted vertically – left part. Screenshot of 2D emittance figure on displayed control panel with computed data – right part.

OPTICAL PROPERTIES

The ions selected by the entrance slit are deflected by an electrostatic deflector composed of two parallel and polarized plates, see Fig. 2. The distribution of the positions of each beamlet is obtained with the measurement of the displacement of the motor. The simple relation in Eq. (1) between the applied voltage (±V), the accelerating potential (U) and the incidence angle (x' noted θ_A) is obtained with the equation of the motion of a charged particle in an uniform electric field and paraxial beam approximation. Simulations are performed with a 3D numerical model in order to assess the performances of the real system with slits and electron repeller limited apertures and fringe field of the deflector.

Table 1: Main Design Parameters

Scan plane	Horiz. or vertic.
Scan speed	Few min. - few hours
Scan length	≤ 123 mm
Resolution in position	100 µm
Resolution in angle	1 mrad
Angular acceptance	+/- 100 mrad
Current intensity	10-3000 µA
Power CW (DC)	≤ 300 W
Emittance normalized	0.01-1 π mm.mrad
Beam transverse envelop	≤ 80 mm in diam.
Time structure	DC or pulsed
Electron repeller	1 kV

ISBN: 978-3-95450-204-2 ISSN: 2673-5350 doi:10.18429/JACoW-IBIC2019-TUPP007

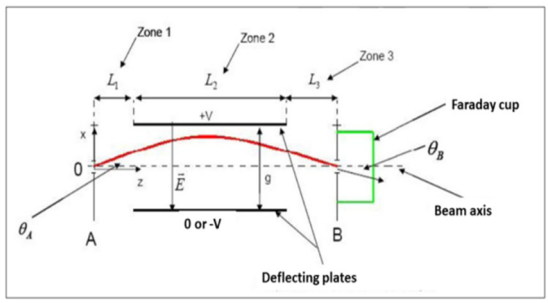

Figure 2: Principle of emittance measurement by incidence angle analysis of the ions sampled by the entrance slit then deflected inside the probe.

$$\Theta_B \approx \Theta_A \approx \frac{\Delta V\ L2\ (L2+2L3)}{4\ U\ g\ (L1+L2+L3)} \qquad (1)$$

With ΔV: Voltage between plates, Θ_A: initial incidence angle, U: beam acceleration potential, g, L1, L2, L3: dimensions.

According to [6] maximum incidence angle should be limited geometrically to ±128 mrad with g=5 mm, L1=L3=4.5 mm and L2=60 mm. This angle defines the angular acceptance of the deflector and corresponds to an accelerating potential of 32.8 kV with maximum operational voltage ΔV=1400 V. The optical properties of the instrument and beam dynamics are assessed by integration of the particle movement into the 3D field map and compared with the formula in Eq. (1), see Fig. 3. Voltage ΔV is proportional to angle Θ, difference between formula and model increases linearly with angle and slightly with initial ion position (off-axis) due to fringe field; for 100 mrad maximum error is 5 %. For small incidence angle error decreases e.g. for 50 mrad it is limited to 1 %. Same effect exists in the transverse horizontal plane as ions are lost on exit slit and repeller for y>39.8 mm due to fringe field produced deviation leading to small collected ion current reduction (<0.5 %). Angular acceptance is ±90 mrad due to beamlet loss on electron repeller, see Fig. 4-5. Another momentum acceptance limitation appears at 60 keV kinetic energy for ΔV=1400 V and ±80 mrad. To reach higher momentum and angle it is required to increase voltage applied on plates.

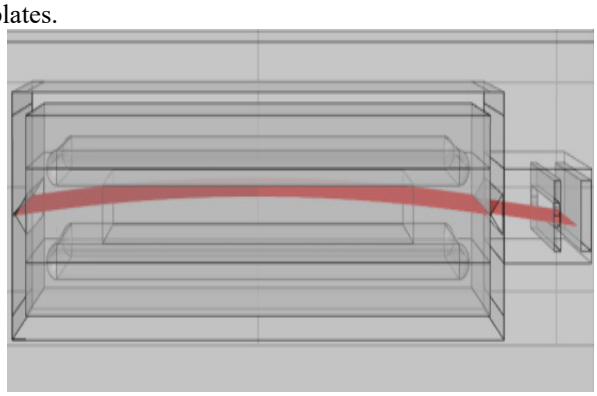

Figure 3: Ion beam tracing between entrance and exit slits with the different aperture reductions as electron repeller and deflecting plates.

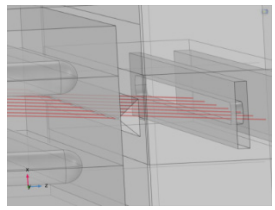

Figure 4: Collection of all ions on Faraday cup.

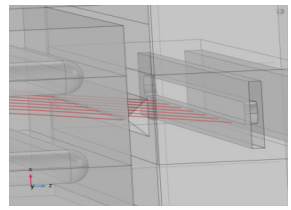

Figure 5: Ions are lost on the electron repeller.

SPACE CHARGE EFFECT

The space charge effect is investigated in stationary case with invariant fields and uncoupled E and B–fields in order to evaluate beam losses and errors on emittance measurement. For high intensity beam e.g. 10 mA beamlet current is assumed to reach 10's µA. At low energy repulsive forces between ions defocuses beam and lead to losses, see Fig. 6. Radial beam expansion factor is > 10 and further developments are required in order to quantify beam losses at exit slit and electron repeller.

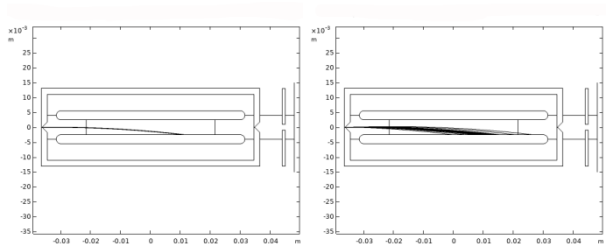

Figure 6: Beam tracing from input to exit slit with electron repeller and Faraday plate on the right part. Without space charge on the left and with space charge on the right side, 15 keV, 100 µA beam. Plates are not polarized.

DEFLECTING PLATES

Interaction of incident ions with metal surface is investigated. Of particular interest is the interaction of heavier ions with the deflector plates in order to verify the production of contaminant beam [8]. Stainless steel plates are composed of 74 % Fe, 19 % Ni and 7 % Cr. Scattering and sputtering increase with large incidence angle (nearly tangential ones). With angle <85° surface emission is significantly reduced. For example with proton backscattering is weak with ≤70° incidences and yield increases for more tangential angles (≥85°) and at lower energy (<100 keV). Sputtering and backscattering increase with incident ion atomic mass. There is poor evidence of sputtering by protons from stainless steel surface. Iron is the most sputtered atom. For nearly tangential incidence (>85°) there are 3.57 sputtered iron atoms per incident ion, see Table 2. Contaminant beam and ghost signal can be produced by tangential ions especially for energy <700 keV and angles >85°.

ISBN: 978-3-95450-204-2 ISSN: 2673-5350 doi:10.18429/JACoW-IBIC2019-TUPP007

Table 2: Sputtering and Scattering with Nitrogen Ions on Stainless Steel Plates (Iron, Nickel and Chromium)

Energy (keV)	700	100
Angle (°)	85	85
Projected range (µm)	0.15	0.05
Backscattering (%)	48.6	61
Sputtering (%)	Cr 38.2, Fe 357, Ni 87.8	0
Distribution (°)	20-150	10-160

SLITS

According to [9] stopping power is weakest for proton beam: at 100 keV estimated range in tungsten is <0.5 µm. Slit thickness is ≥0.3 mm (trapezoidal shape) and therefor aperture enables an accurate sampling of the beam. Nevertheless perpendicular contact surface doesn't favor heat dissipation thus compromise is necessary to limit backscattering. Surface emission decreases with incident ion energy and increases with atomic number. Angular distribution is a relevant criterion of the slit design and contaminants reduction (due to contact angle with beam).

A significant part of beam is stopped at the entrance slit, leading to heat loading. Taking tungsten as the material of the slit, the melting temperature is 3400 °C. It is obvious that the smaller the slit aperture the higher the resolution and the lower the signal amplitude. Since the thickness of the slit decreases the angular acceptance a trapezoidal shape of slit is adopted.

IN-FIELD USE AND ACTIVATION

The in-field use and the need to share between different labs lead us to consider the safety issues related to staff and transport as equipment will be submitted to radiation and activation. Radiation field around high energy accelerator, input data for simulations of activities, equivalent dose rate (EDR) and cooling times are considered. The model is composed of slits, deflector, electron repeller, Faraday cup, external shield, thermic screen, cooling circuit with water, actuator, vacuum tube, cave in concrete and surrounding air. Simulations of isotope production are performed with Monte Carlo code FLUKA [10] via high energy processes, low energy neutron interactions, transport thresholds, and neutrons down to thermal energies (no electromagnetic cascade was simulated). Calculated quantities are: radioactive isotope production and decay for specific irradiation and cooling patterns including radioactive daughter products and coupling between materials.

Neutrons produced by high energy heavy ions interaction with environment present two characteristic spectra: evaporation neutrons (<10 MeV, isotropic distribution) and cascade neutrons (E < acceleration energy, continuous spectrum). Secondary neutrons are produced along the beam line, in the walls and in target. According to Brassart [11]: 50 % of EDR is due to neutrons in the range of 0.1 - 10 MeV, 10 – 20 % to low energy neutrons and gamma radiation, and complements due to neutrons at energies >10 MeV. Intra-nuclear cascades start to be important at energies >50 MeV. Irradiation sources due to beam losses are distributed according to 5 % inside cyclotron and 10 % during transport.

Simulations confirm that no significant activation is produced by direct low energy beam irradiation, Fig. 7-8. Due to secondary neutron radiation fields prompt equivalent dose is < 10^{-5} Sv, Fig. 9-10. Some radionuclides with long life time request further investigation in order to enable easy transportation as: ^{179}Ta (1.82 y), ^{3}H (12.32 y), ^{55}Fe (2.737 y). In-field secondary neutron radiation field measurement and activation of samples will complete MC simulations and deliver additional data for final safety demonstration.

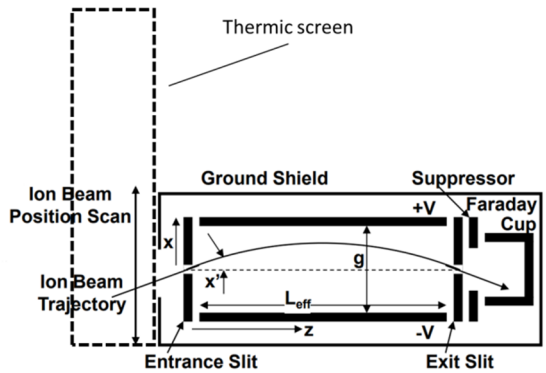

Figure 7: Model used for radioactive isotope production calculation is composed of slits, deflector, electron repeller, Faraday cup, external shield, thermic screen, cooling circuit with water, actuator.

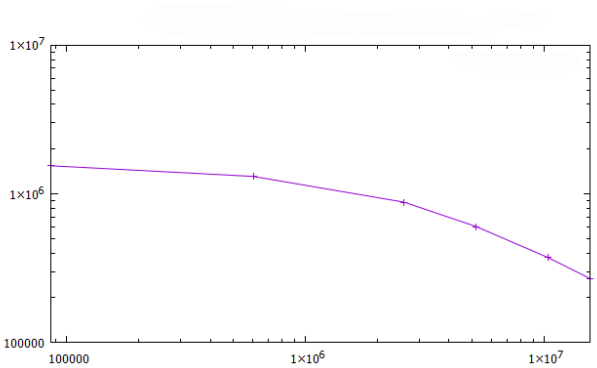

Figure 8: Activity decay in the tungsten slit at the entrance of the probe (Bq).

ISBN: 978-3-95450-204-2 ISSN: 2673-5350 doi:10.18429/JACoW-IBIC2019-TUPP007

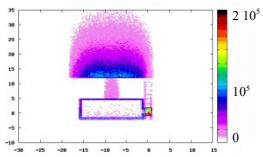

Figure 9: Prompt activity after one week (Bq/cm3).

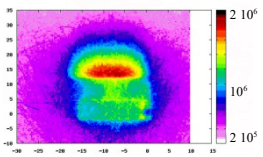

Figure 10: EDR after one week (pSv).

DISCUSSION AND PERSPECTIVES

According to calculations performed with complete 3D model of emittance-meter probe error relative to angular incidence definition with currently used formula is ≤5 %. The error induced by small reduction of collected ion current on Faraday cup is produced by the necessary aperture limitations along the beam path. Effect on emittance measurement accuracy remains negligible for most standard in-field beam characterizations. Beam halo current intensity measurement appears possible by increase of voltage applied on deflecting plates. This will enable measurement of higher incidence angles thus higher acceptance of collected ions. Verification of dielectric rigidity in the deflector area and range of beam rigidity regardless of position in transverse plane is required. Space charge effect between entrance slit and Faraday cup has been identified as a potential source of beam losses and requires more investigations. Those issues are of particular interest to increase the performances of the system. On the other hand experiments are foreseen with ion beams in order to confirm thermal behavior of irradiated parts at the entrance of the emittance-meter. Secondary neutron radiation field measurement and activation of samples in accelerator environment will complete MC simulations. Those developments are justified by demands towards higher acceptance and smaller losses for high power accelerators and high intensity radioactive beams.

ACKNOWLEDGEMENTS

Author acknowledges the contribution of colleagues who made the work easier by bringing new ideas and recalling “old stories”, among them F. Bulteau-Harel, G. Claus, H. Dieumegard, R. Duchêne, G. Febvre, R. Ferdinand, C. Gradziel, M. Heine, C. Illinger, V. Juste, Y. Le Gall, S. Mitrofanov, Y. Patois, F. Poirier, T. Thuillier, O. Tuske, as well as the beam instrumentation network, the RIF at IN2P3.

REFERENCES

[1] R. Ferdinand *et al.*, “Final Results of the SPIRAL2 Injector Commissioning”, in *Proc. 10th Int. Particle Accelerator Conf. (IPAC'19)*, Melbourne, Australia, May 2019, pp. 848-851. doi:10.18429/JACoW-IPAC2019-MOPTS006

[2] R. Ferdinand *et al.*, “Status of SPIRAL2 and RFQ Beam Commissioning”, in *Proc. 28th Linear Accelerator Conf. (LINAC'16)*, East Lansing, MI, USA, Sep. 2016, pp. 668-672. doi:10.18429/JACoW-LINAC2016-WE1A06

[3] F. Gougnaud *et al.*, “The Implementation of the Spiral2 Injector Control System”, in *Proc. 13th Int. Conf. on Accelerator and Large Experimental Control Systems (ICALEPCS'11)*, Grenoble, France, Oct. 2011, paper MOPMU025, pp. 491-493.

[4] O. Tuske et al., “Commissioning of the ECR ion source of the high intensity proton injector of the Facility for Antiproton and Ion Research (FAIR)”, RSI 89, 052303 (2018).

[5] O. Tuske *et al.*, “Commissioning of the High Intensity Proton Injector of the Facility for Anti Proton and Ion Research at CEA-Saclay”, in *Proc. 22nd Int. Workshop on ECR Ion Sources (ECRIS'16)*, Busan, Korea, Aug.-Sep. 2016, pp. 86-88. doi:10.18429/JACoW-ECRIS2016-WEPP02

[6] P. W. Allison et al., An emittance scanner for intense low-energy ion beams, IEEE Transactions on Nuclear Science, Vol. NS-30, No. 4, 1983.

[7] J. Schwedt, Etude et réalisation d’un émittance-mètre basse-énergie pour mesure en ligne et contrôle faisceaux, Ph.D thesis, thèse de l’université de Strasbourg, 1983.

[8] MP. Stockli, Ghost signals in Allison emittance scanners, FERMILAB-CONF-04-510-AD, 2004.

[9] J. F. Ziegler and J. P. Biersack, SRIM - The stopping and range of ions in solids, 1985.

[10] V. Vlachoudis, Proc. Int. Conf. on Mathematics, Computational, Methods & Reactor Physics (M&C 2009), Saratoga Springs, New York, 2009.

[11] N. BRASSART et al., Aspects spécifiques de la radioprotection autour d'un cyclotron, Radioprotection, Les Editions de Physique, Vol. 30 n° 3, 1995, pp. 411-422.